Study of MILD combustion using LES and advanced analysis tools

Zhiyi Li[a,*], Stefanie Tomasch[a,b], Zhi X. Chen[a], Alessandro Parente[c], Ivar S. Ertesvåg[b], Nedunchezhian Swaminathan[a]

[a]*Cambridge University, Engineering Department, Hopkinson Lab, Trumpington Street, Cambridge CB2 1PZ, UK*
[b]*Norwegian University of Science and Technology, Department of Energy and Process Engineering, NO-7491 Trondheim, Norway*
[c]*Université Libre de Bruxelles, Ecole polytechnique de Bruxelles, Aero-Thermo-Mechanics Laboratory, 1050 Brussels, Belgium*

Abstract

A cylindrical confined combustor operating under MILD condition is investigated using LES. The combustion and its interaction with turbulence are modeled using two reactor based models, PaSR and EDC. Results show that the Partially Stirred Reactor (PaSR) model yields improved estimation for mean temperature and species mole fractions compared to Eddy Dissipation Concept (EDC). LES data are analysed using advanced post-processing methods such as the chemical Tangential Stretching Rate (TSR), balance analysis and local Principle Component (PCA) analysis. TSR can identify chemical explosive (ignition-like) and contractive (burnt) regions. With the balance analysis of the convective, diffusive and reactive terms in temperature equation, regions with substantial heat release coming from ignition or flame are identified. The local PCA analysis classifies the whole domain into clusters (regions with specific features) and provides the leading species in each cluster. The three analyses correlate well with one another and it is observed that the most chemically active region locates upstream

*Corresponding author: zl443@cam.ac.uk

(in the near-field). Also, both autoignition and flame-like structures play equally important roles in MILD combustion.

1. Introduction

More than 90% of the world total primary energy supply comes from combustion in one form or another. There are challenges to meet future energy requirement because of the limited fossil fuel resources. Also, the impact of combustion on the environment through emissions of green house gases, CO_2, and pollutants such as NO_x and soot is well-known. Hence, developing efficient combustion technologies with low emissions and fuel flexibility has become imperative. Moderate or Intense Low oxygen Dilution (MILD) combustion is a very promising technology and requires a massive recirculation of exhaust gases within the reaction region [1, 2]. The hot exhaust gas preheating reactants helps to stabilize combustion and minimise hotspots, which yields a uniform temperature field and suppresses combustion noise [1]. Also, the temperature rise across the combustion zone is only few tens of Kelvin above the background hot gas temperature, typically below 1800 K, inhibiting production of thermal NO_x, CO and soot [1, 2].

Various lab-scale burners have been used in experimental studies, including the Jet in Hot Coflow (JHC) burner [3, 4], reversed-flow arrangement having the inlet and outlet on the same side [5] and cylindrical combustor with a converging duct towards the outlet [6]. The effect of hot gas recirculation is included in JHC configuration by using combustion products of an upstream burner. However, this configuration does not account for the effect of internal recirculation as it happens

2

in realistic industrial systems. It is therefore not considered in the current study. The geometry of the other two configurations inherently include the recirculation of hot gases. More spatially uniform temperature field was observed in these configurations compared to JHC case. Also, the combustor in reversed-flow case was well-insulated, but the case in [6] allows heat loss through the wall, which could influence the combustion stability. Hence, conditions achieved in [6] are expected to be representative of practical MILD combustion conditions and thus, this burner is of interest here.

Large Eddy Simulation (LES) using a three-stream Flamelet Progress Variable (FPV) formulation was used in [7] to model the JHC flame. This burner was also studied using Partially Stirred Reactor (PaSR) [8] and laminar chemistry (without turbulence-chemistry interaction effects) [8] in the context of LES. All of these studies showed good agreement with measurements. The other two enclosed cases have also been investigated in past studies using tabulated chemistry approaches. The FPV involving counter-flow diffusion flames was extended to include the dilution effects in [9] and a diluted homogeneous reactor was used in [10]. Both of these approaches use tabulated chemistry and provided results in good agreement with the experimental data. These approaches involve a multi-dimensional lookup table, whose generation is quite tedious and time consuming. Reactor-based models such as PaSR and EDC do not require to consider dilution explicitly since the chemical species of interest (involved in the kinetic mechanism used) are transported. Depending on the size of the chemical mechanism, these methods can be more computationally expensive, compared to tabulated chemistry.

The objectives of the present study are (i) to conduct LES of MILD combustion in experiment [6] using the PaSR and EDC models for subgrid scale (SGS)

combustion, (ii) to analyse the LES data using Computational Singular Perturbation (CSP) [11] and balance [12, 13] analyses to identify autoignition and flame regions, and (iii) to apply local Principal Component Analysis (PCA) [14] to extract potential chemical markers for these regions. We believe that this is the first direct comparison of PaSR and EDC models for MILD combustion in a combustor with strong internal recirculation zones simulated using LES paradigm. Most importantly, the advanced data analysis tools reveal intriguing features of MILD combustion, providing impetus to further numerical and experimental investigations.

This paper is organised as follows. The test case and its numerical modelling are described in sections 2 and 3 respectively. The SGS combustion models are described briefly in section 4 and the results are discussed in section 5. The analyses to identify autoignition and flame regions are discussed in section 6 and conclusions are summarised in the final section.

2. Experimental Configuration

A 10 kW lab-scale MILD combustor investigated in [6] is chosen as the test case for this study. This cylindrical combustor operating at atmospheric pressure has air at 673.15 K entering through a central jet of diameter d_a = 10 mm with a bulk-mean velocity of U_a = 113.2 m/s, giving a Reynolds number of 17526. Methane at 298.15 K is injected into the combustor through 16 jets with d_f = 2 mm and U_f = 6.2 m/s. The cylindrical combustor has a diameter of 100 mm for a length of 340 mm and then it converges at 15°, as shown in Fig. 1. A strong recirculation region with hot flue gases is achieved aerodynamically because of the converging section.
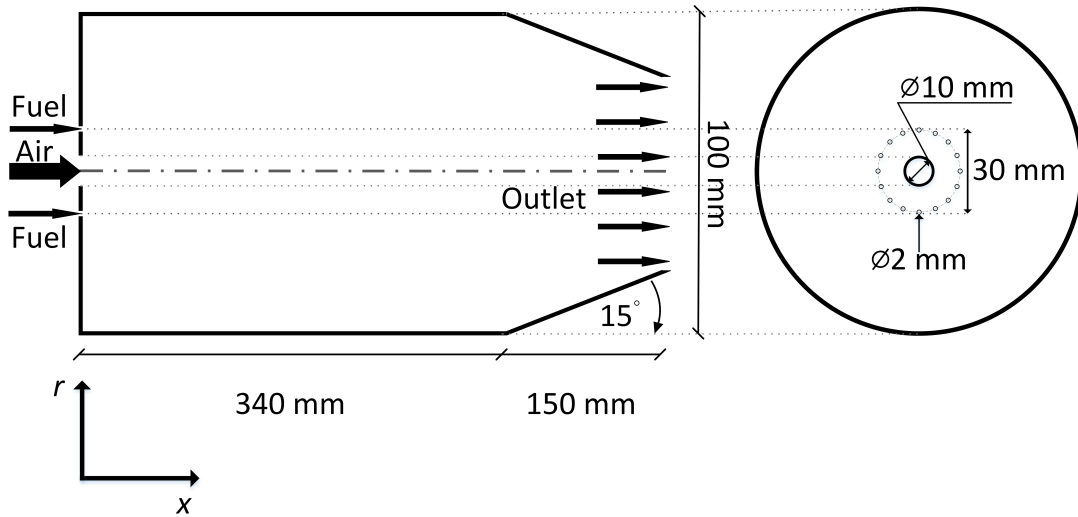
Figure 1: Schematic view of the combustor geometry [6].

Several experiments were conducted in [6] with an excess air ratio in the range of $1.1 \leq \lambda \leq 2.2$. Among these various experimental cases, the case labelled RUN2 with $\lambda = 1.3$ is under MILD condition and it is selected for this study. Detailed measurements of mean temperature, dry mole fractions of O_2, CO_2, HC, NO_x and CO are reported in [6]. The mole fractions are measured using stainless steel water-cooled sampling probes (average repeatability of data within 10%) and local mean temperature measurements were obtained using 13% rhodium (type R) thermocouples with uncertainty less than 5% [6]. The radial variations of these quantities are reported in [6] for several axial locations in the non-converging section of the combustor.

3. Numerical Set-up

The schematic shown in Fig. 1 forms the cylindrical computational domain and it is discretised using O-grid. Three different grids having 2, 4, and 8M

5

cells are considered. The flow rates at the inlet are specified to match the conditions of the fuel and air streams. Since the fuel jet Reynolds number is small, no turbulence is specified but the air stream turbulence is specified using a synthetic turbulence [15] based inflow generator. The RMS velocity for air stream is u_{rms} = 20 m/s, following an earlier study [10] and the length scale specified for the inflow generator is 5.5 mm, 55% of jet diameter. Mean top-hat profiles without fluctuation are used for inlet scalar boundary conditions. The no-slip walls are specified to be at 1000 K based on previous studies [9, 10]. The boundary layers are unresolved and represented with wall functions. All the scalar and velocity gradients in the direction normal to the outlet plane are specified to be zero. The simulations are run for $21\tau_{\text{flow}}$, where τ_{flow} is the flow through time for the entire combustor length based on U_a. The statistics are collected over the last $8\tau_{\text{flow}}$ after allowing the initial transients to leave the combustor. First, a non-reacting flow is simulated using OpenFOAM-2.3.0 [16] software and the above three grids. This code solves Favre-filtered mass, momentum, and energy conservation equations along with filtered transport equations for scalars required in combustion modelling. The sub-grid stresses are modelled using one equation (for SGS kinetic energy, $\mathcal{K}$) model with constant coefficient. Simulation results from the three grids are included in the supplementary material. Detailed analysis of the non-reacting flow results showed that more than 80% (indeed 90% in regions of scalar mixing and combustion) of the turbulent kinetic energy is resolved using the mesh with 2M cells. Moreover, past DNS studies [12] of MILD combustion showed that the reactive structures are broader than Kolmogorov scales and using grid spacing of 3 to 5 times the laminar thermal thickness is sufficient for a good LES. In the current case, the estimated laminar thermal thickness [12] is 0.36 mm. The

cell size of the 2 M grid ranges from 0.27 to 1.8 mm. Thus, this mesh is appropriate for the current MILD combustion simulation. The edcSMOKE [17] finite rate chemistry solver is used for the PaSR and EDC sub-grid (SGS) combustion models, briefly described in the following.

4. Combustion Models

Methane-air combustion chemistry is modelled using a skeletal mechanism [18], which was shown to be adequate for MILD conditions in [13] and in [8, 19]. For the finite-rate based LES of a combustion with the current geometry, such mechanism is considered to be the best to balance between CPU hour requirement and accuracy. Both PaSR and EDC assume that each computational cell consists of a reactive structure and a surrounding fluid. Combustion occurs in the reactive structure while surrounding fluid accounts for scalar mixing processes. These mixing processes can be imperfect in turbulent combustion and thus the filtered reaction rate, $\overline{\dot{\omega}}_k$ required for the scalar transport equation is specified using $\overline{\dot{\omega}}_k = F \cdot \dot{\omega}_k^*(\widetilde{Y}, \widetilde{T})$, where $\dot{\omega}_k^*(\widetilde{Y}, \widetilde{T})$ represents the reaction rate of species k in the reactive structure. The reactive structure reaction rates are estimated by solving a canonical reactor, typically a perfectly stirred reactor (PSR) or a plug flow reactor (PFR). The residence time in the canonical reactor for this study is set to be CFD time step [8]. The term F in the above equation represents the fraction of the reactive structure in a numerical cell and its detail depends on the modelling approach used.

7

4.1. Partially Stirred Reactor model

The reactive fraction F for the PaSR model, typically denoted using κ [20], is calculated as

$$F \equiv \kappa = \frac{\tau_c}{\tau_c + \tau_{\mathrm{mix}}}, \tag{1}$$

where τ_c and τ_{mix} are the characteristic chemical and mixing time scales respectively in a cell. Here, the chemical time scale for species k is estimated as $\tau_{c,k} = Y_k^*/\left(dY_k^*/dt\right)$, which is obtained from a PFR solution. The symbol t denotes the time. The maximum value of $\tau_{c,k}$ (removing the dormant species) is chosen as τ_c [21]. The mixing time scale is defined as $\tau_{\mathrm{mix}} = \sqrt{\tau_\Delta \tau_\eta}$, where $\tau_\Delta \simeq \Delta/\sqrt{\mathcal{K}}$ is the SGS flow time scale and $\tau_\eta \simeq \sqrt{\nu/\epsilon_{sgs}}$ is the SGS viscous time scale [8]. The symbols Δ and ϵ_{sgs} denote the LES filter width and SGS dissipation rate of $\mathcal{K}$.

4.2. Eddy Dissipation Concept model

EDC is based on turbulent kinetic energy cascade [22]. This provides the fraction of the reactive structures F in the flow [22], as:

$$F = \frac{\gamma_\lambda^2}{1 - \gamma_\lambda^2}, \tag{2}$$

with γ_λ estimated as a function of the flow characteristic scales:

$$\gamma_\lambda = C_\gamma \left(\frac{\nu \epsilon_{sgs}}{\mathcal{K}^2}\right)^{1/4}. \tag{3}$$

The model constant $C_\gamma = 2.1377$ is taken from a RANS study [22] as a first approximation.

Compared to PaSR model, EDC utilises only fluid mechanical time scales, more precisely it involves a ratio of molecular to SGS eddy viscosities, without involving a chemical time scale to evaluate F.

8

5. Results and Discussion

5.1. Streamline profiles

The time-averaged streamline profiles on the mid-plane for the two models are shown in Fig. 2, marking the recirculation zones. There are mainly two recirculation zones. The smaller one is located at the side corner ($|r| \geq 0.02$ m, x ≤ 0.05 m) and the larger one, which brings the hot flue gases upstream and heats up the fresh air and fuel mixture, is established in the middle of the domain. Compared to PaSR model, the centre of the large recirculation zone from the EDC is situated more downstream, at around $x = 0.17$ m, while it is at about $x = 0.1$ m for PaSR. Since the same boundary conditions are used for both models, the differences in the streamlines come from combustion effects, showing that the most reactive region for EDC is probably located further downstream than that for PaSR.
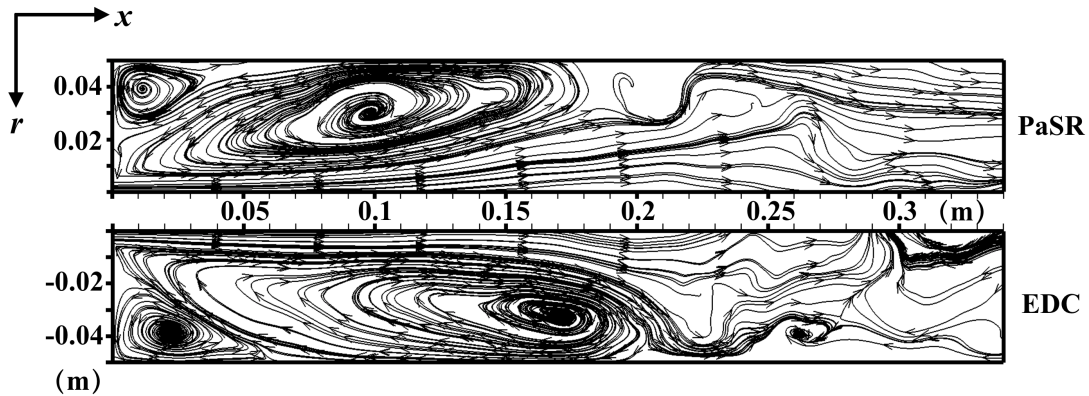

Figure 2: Streamline profiles from PaSR and EDC combustion models

5.2. Comparisons with measurements

Figure 3 shows the time-averaged temperature fields obtained from the LES using the PaSR and EDC models along with experimental results taken from [6].

9

The symbols in the experimental frame show scalar probe measurement locations. Overall, a reasonable agreement with experimental profile is observed for the PaSR model. However, the penetration of the air jet is over estimated (0.1 m compared to 0.079 m in the experiment) which could be related to the turbulence conditions specified at the air stream inlet. The incoming turbulence and boundary layer at the lip will influence the jet spreading angle and these affect the near-field behaviour, which is also apparent in the results. The high temperature region predicted by the PaSR model spans between $x = 0.1$ m and 0.25 m, while this region extends up to $x = 0.3$ m in the experiment. Hence under-prediction of temperature is anticipated after $x = 0.25$ m. The general pattern of the temperature variation predicted using the EDC is similar to that obtained using the PaSR model but the temperature values are under-predicted by the model as seen in Fig. 3. At $x = 0.11$ m, the PaSR model shows a large temperature gradient while, for EDC, the temperature increase is located at around $x = 0.185$ m. These locations correlate with the centre of the large streamlines accounting for flue gas recirculation in Fig. 2.
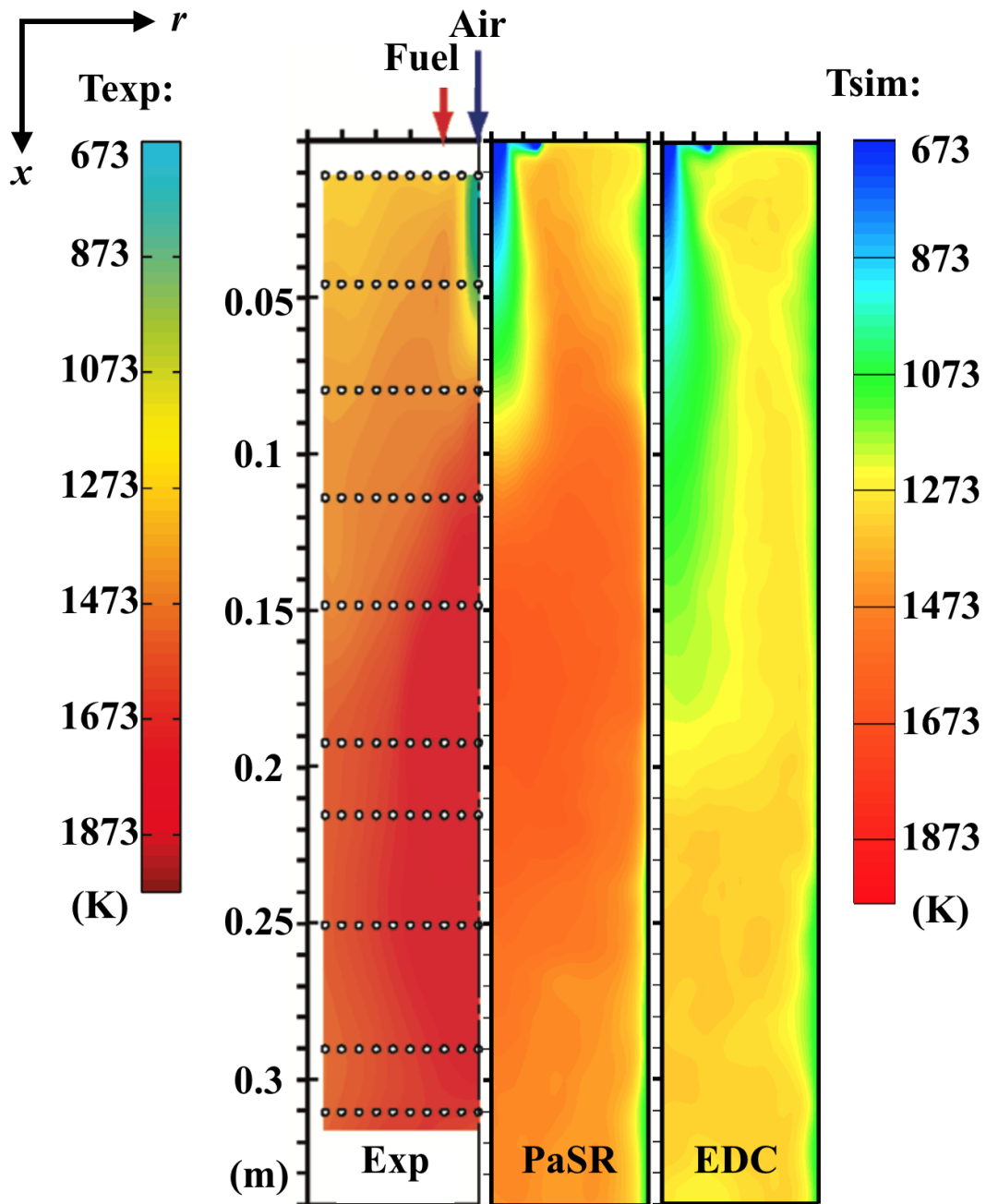
Figure 3: Averaged temperature fields in the mid plane for PaSR and EDC models and measurements.

The measured temperature field shows a strong radial gradient for $x \leq 0.15$ m which is also represented in the computational results. For further evaluations, the axial locations of x = 11/45/79/113/147/310 mm are considered.

The radial variations of mean temperature computed using the PaSR and EDC models are compared to the experimental data in Fig. 4. The results are shown for six axial locations. The EDC under-predicts temperature in general as observed in the previous figure. The values computed using the PaSR model compares quite well with the measurements and this comparison is similar to those obtained in [9, 10]. However, the average temperatures at x = 310 mm is underestimated by about 200 K. On the other hand, earlier studies [9, 10] showed an overestimation by about 150 to 200 K.
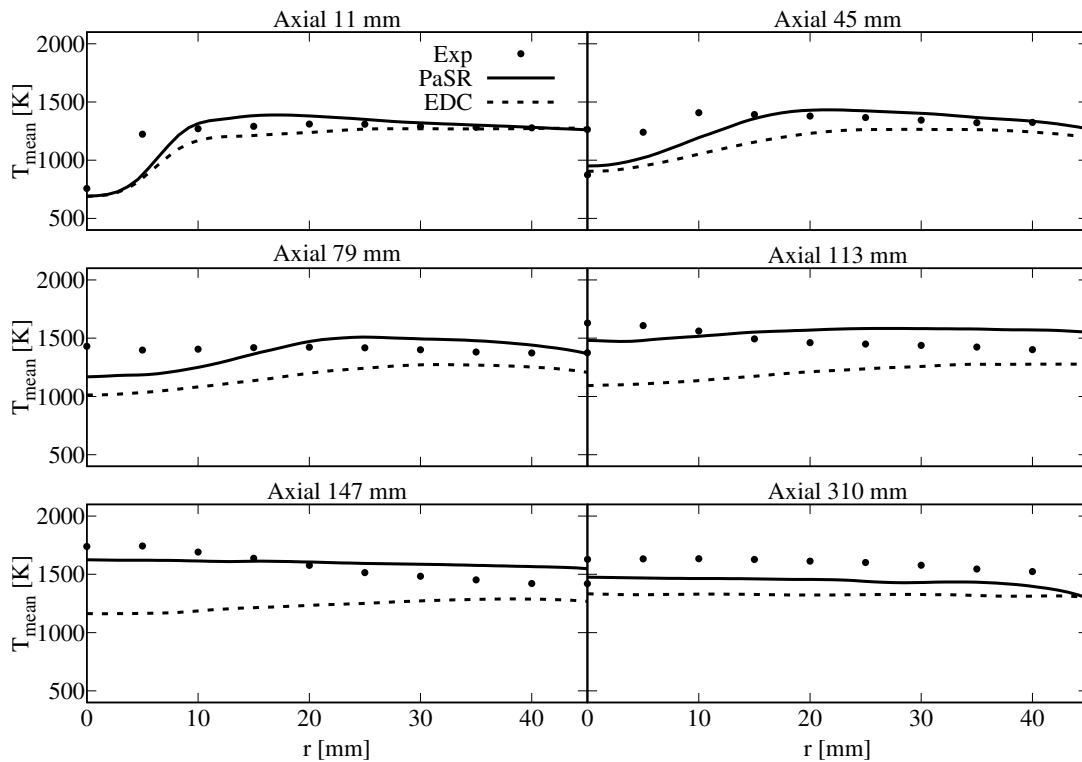
Figure 4: Comparison of computed and measured radial variation of mean temperature at six axial locations.

The species mole fraction for O_2 and CO_2 are shown in Figs. 5 and 6. The computed values of these species mole fractions compare quite well with experimental data for the location $x = 11$ mm and the difference between the PaSR and EDC models is small. The difference between the models' prediction increases as one moves downstream with almost no difference for $x = 310$ mm, where the equilibrium values are expected. A closer scrutiny of the results in these two figures show a substantial difference between the computed and measured mole fractions for the first three experimental data points of $r \leq 10$ mm at $x = 45, 79, 113$ and 147 mm, which is also consistent with earlier studies using different combustion

13

models [9, 10]. For the incoming air and fuel stream temperatures, one would expect relatively higher CO_2 values and O_2 mole fractions substantially lower than 0.2 in the regions with temperature larger than about 1100 K. The experimental data seem to contradict this and a simple energy balance analysis discussed in the supplementary material suggests that there might be some issues in the measurements of CO_2 and O_2 mole fractions in the regions noted above. For these reasons, these specific experimental data points are excluded while evaluating the overall model performance. To conclude, the species mole fraction are well predicted for $x = 11$ mm by both PaSR and EDC models. After $x = 45$ mm, EDC under and over predicts CO_2 and O_2 respectively. The PaSR model works well across the whole domain if one excludes the specific data points noted above.
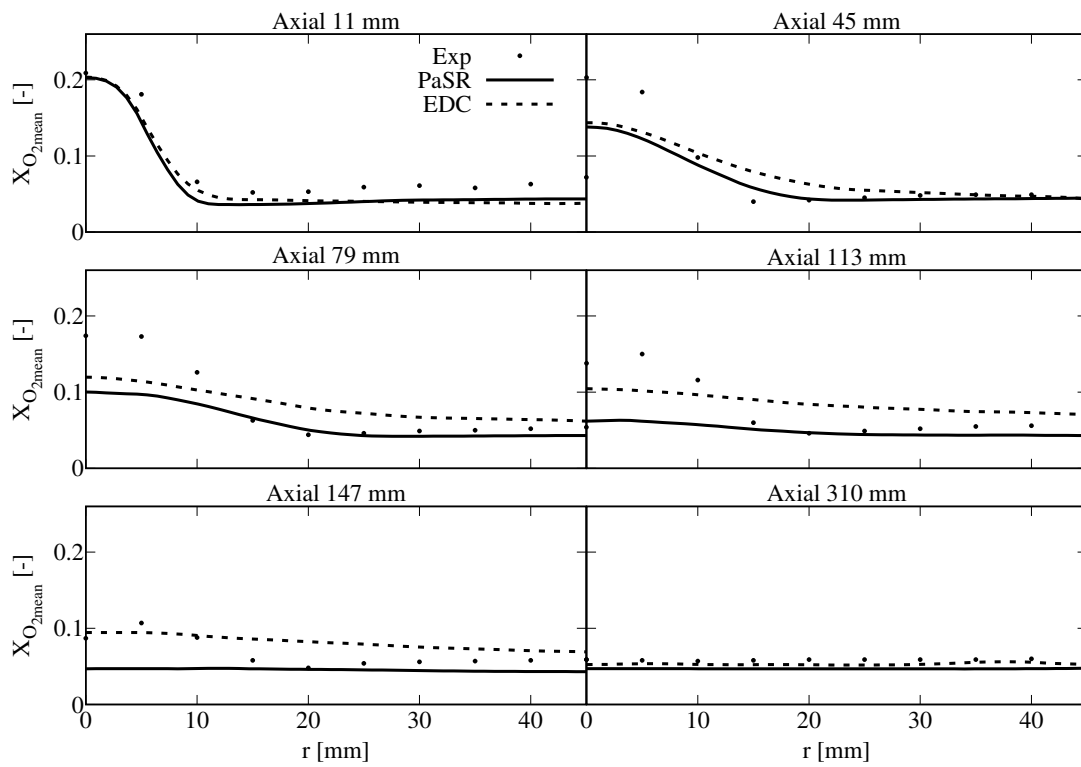
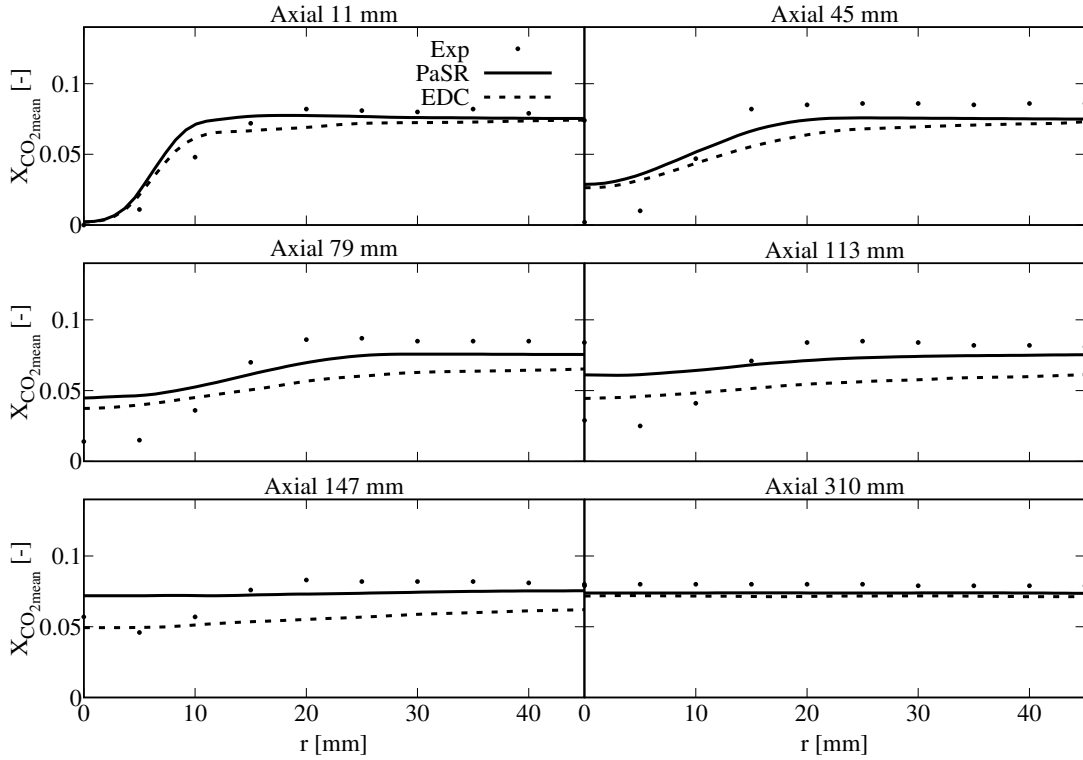Figure 5: Comparison of computed and measured mean O_2 mole fraction for six axial locations.

Figure 6: Comparison of computed and measured mean CO_2 mole fraction for six axial locations.

6. Analysis of Reaction Zones

6.1. Analysis methods

Three methods, CSP, a balance analysis and local PCA, are used to extract information required to identify ignition- and flame-like regions in MILD combustion. These methods are explained briefly below before presenting the results.

6.1.1. TSR obtained from CSP analysis

The general form of species and energy equations in a homogeneous reactive system can be expressed with $\partial z/\partial t = g(z)$, where $g(z)$ is the chemical source vector and z is N dimensional state vector including N_s, the species mass fractions

16

and temperature: $N = N_s + 1$. The chemical source vector can also be written using a new set of basis vectors $\boldsymbol{a}_i(z)$, with $\boldsymbol{g}(z) = \sum_{i=1}^{N} \boldsymbol{a}_i(z) f^i(z)$, where $f^i(z)$ is the amplitude of the i-th mode. The term $f^i(z)$ can be further expressed as $f^i(z) = f^i(\boldsymbol{g}(z)) := \boldsymbol{b}^i \cdot \boldsymbol{g}(z)$ and $\boldsymbol{b}^i$ denotes the dual basis vector. The bi-orthonormality condition allows to recover the original representation of $\boldsymbol{g}(z)$. Based on CSP, the basis vectors $\boldsymbol{a}_i$ and covectors $\boldsymbol{b}^i$ can be approximated to leading order, by the right and left eigenvectors of the Jacobian $\boldsymbol{J_g}$ of $\boldsymbol{g}(z)$, respectively. This set of basis vectors is traditionally employed in CSP [11] to decouple local time scales $\tau^i = 1/\lambda_i$, where λ_i are the eigenvalues of Jacobian $\boldsymbol{J_g} = |\partial \boldsymbol{g}/\partial z|$.

The tangential stretching rate (TSR) denotes the level of stretching or contraction of the dynamics of interest along the direction of a vector field and is used here to characterize the most *energy-containing* time scales developing in the chemically reactive system of interest here [23, 24]. This method was used for turbulent premixed flames [25] and MILD flames [19] in previous studies. The stretching rate of the reactor dynamics in the direction tangential to the vector field $\boldsymbol{g}(z)$ is $\omega_{\tilde{\tau}}(\boldsymbol{g}) := \sum_{i=1}^{N} W_i(\boldsymbol{g}) \, \lambda_i$, with λ_i as the eigenvalue of i-th mode. The weight, W_i, is

$$W_i(\boldsymbol{g}) := \frac{h^i(\boldsymbol{g})}{|\boldsymbol{g}|} \sum_{k=1}^{N} \frac{h^k(\boldsymbol{g})}{|\boldsymbol{g}|} \, (\boldsymbol{a}_k \cdot \boldsymbol{a}_i). \tag{4}$$

It follows that $\omega_{\tilde{\tau}}$ is essentially a time scale obtained as a weighted average of all *energy-containing* time scales with the weight depending on the mode amplitude associated with that scale. The magnitude of the TSR represents the reciprocal of the most energy containing time scale of the system, while the positive and negative sign of TSR, $\omega_{\tilde{\tau}}$, indicates an explosive (tendency to react) or non-explosive/dissipative nature of the dynamics respectively.

6.1.2. Balance analysis

The balance analysis considers $\mathcal{B} = |C - D| - |R|$, where C, D and R are the convective, diffusive and reactive terms in a species or temperature transport equation [12, 13]. This quantity varies spatially and $\mathcal{B} < 0$ signifies reaction dominated (ignition-like) regions, $\mathcal{B} = 0$ represents flame-like region because of convective-diffusive-reactive balance and $\mathcal{B} > 0$ identifies unburnt or burnt (convective-diffusive) regions. This analysis was developed and used in past studies of MILD combustion [12, 13] and it is used here along with TSR analysis to gain further insights.

6.1.3. local PCA

Principal Component Analysis (PCA) [26] is a statistical technique often used for size reduction. It detects the directions which are most active in a multi-dimensional data set, providing a mathematical formulation to select optimal parameters representing the local thermochemical state.

For a data set, X, consisting of n observations of p variables, the Principal Components (PCs), Z, are defined by the projection of the original data onto the eigenvectors, A, of the covariance matrix, S, $Z = XA$. The eigenvalue matrix, L associated to S quantifies the relative importance of the PCs. Thus a reduced subset of PCs with size q is defined: $Z_q = XA_q$. Such approach minimizes the amount of information loss in the dimension reduction. Each PC is a linear combination of the variables, with weights defined by the covariance matrix eigenvectors. The global PCA analysis cannot handle highly non-linear systems, like turbulent reacting systems. Such realization has prompted the development of a local PCA approach, which employs a partition of the data set into clusters (regions), followed by the local application of PCA in each cluster [14]. Details about the

18

application of local PCA are presented in [14].

6.2. Insights gathered

The above tools are used on the data from the PaSR model, since both instantaneous and time-averaged values of κ in Eq. (1) approach almost 1 in regions of high heat release across the whole domain. The TSR values are obtained using CSPTk software toolkit and the values of $\mathcal{B}$ are normalised using $(\Delta T \rho_r S_L/\delta_{th})$ for stoichiometric methane-air flame with reactants conditions used in the experiment. Figure 7 shows typical variation of $\psi_{\tilde{\tau}} = (|\omega_{\tilde{\tau}}|/\omega_{\tilde{\tau}}) \log |\omega_{\tilde{\tau}}|$ in the mid-plane at an arbitrarily chosen time as a color map. Two more time moments are analysed and results show similar distributions. The snap shots are included in the supplementary material. The regions with high heat release rate, $\widetilde{\dot{Q}}$, are marked using two contours for $\widetilde{\dot{Q}} = 10^8$ and 10^7 W/m^3. The contours of normalised $\mathcal{B}$ are shown for three values to mark flame-like ($\mathcal{B}^+ \sim 0$), ignition-like ($\mathcal{B}^+ < 0$), and convective-diffusive regions. These contours for $x > 0.2$ m are not shown since combustion is almost complete by this axial location, see Fig. 3. Values of $\psi_{\tilde{\tau}} > 0$ indicate the tendency for the local mixture to react and this occurs before ignition begins. Large positive $\psi_{\tilde{\tau}}$ appears close to the shear layer between the air and fuel stream in the near-field. There is no substantial heat release in these region and $\mathcal{B}^+$ is positive. All of these signify convective-diffusive region which is consistent with expectation based on physical considerations. This region is also seen to be intermittent (see the difference between the top and bottom shear layers) because of the strong shear generated turbulence in these areas.
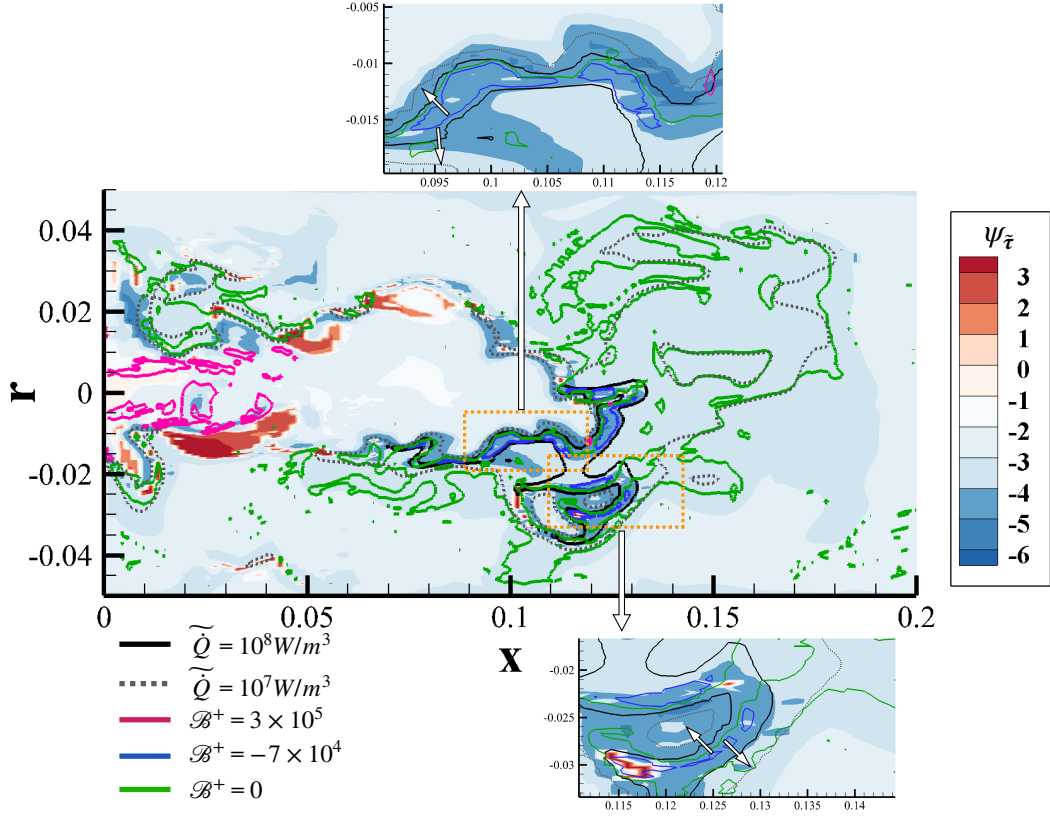
19

Figure 7: Typical distribution of $\psi_{\tilde{\tau}} = (|\omega_{\tilde{\tau}}|/\omega_{\tilde{\tau}}) \log |\omega_{\tilde{\tau}}|$ in the mid-plane is shown along with heat release rate $\widetilde{\dot{Q}}$ and $\mathcal{B}^+$ contours. The unit of the axes is m.

After $x = 0.05$ m, larger negative $\psi_{\tilde{\tau}}$ values appear. Heat release rate larger than 10^7 W/m³ is observed in the regions where $\psi_{\tilde{\tau}}$ changes from positive to negative values (see the location at about $x = 0.05$ m and $r = -0.01$ m). The $\widetilde{\dot{Q}}$ increase to 10^8 W/m³ by about $x = 0.1$ m where $\psi_{\tilde{\tau}} < 0$ start to appear suggesting that the ignition has occurred and these regions are dominated by reactions. Indeed, the values of $\mathcal{B}^+$ are negative suggesting that these are reaction dominated regions. To see these phenomena clearly, these regions are magnified in the insets of Fig. 7 depicting that negative $\mathcal{B}^+$ appears in the middle of the $\widetilde{\dot{Q}}$ contour of 10^8 W/m³,

20

and it expands in the direction of relatively lower $\widetilde{Q} \left(10^7 \ \text{W/m}^3 \right)$, indicated by the white arrows. Hence, it is clear that the MILD combustion shares some conventional combustion features while having its own distinctive attributes, as observed in past DNS studies [12, 13], which can be captured using the PaSR model.

From Fig. 7, different areas with varied features are identified. In order to better characterize the current flame with region-based post-processing tool, local PCA approach [14] is used here. In total eight clusters are used, each one representing a specific area of the system (see Figure 8). In each cluster, one species contributing the most (showing the highest weight) to the first PC is identified. It is observed that cluster 2 marked with OH is located in the region where $\mathcal{B}^+ = 0$ and $\widetilde{Q} = 10^7 \ \text{W/m}^3$. This area represents the flame region, which is consistent with the identification of a flame marker such as OH as principal variable. The region with positive $\psi_{\tilde{\tau}}$ value indicates the explosive region of the flame, where the radical pool (H, O and OH) is initiated, before ignition takes place. Cluster 5 in this region is characterised by H (followed by O) as the most contributing species, which is again consistent with what is observed in Fig. 7. H_2O_2 is the leading species in cluster 8. This area overlaps with the region showing high heat release, as well as negative $\psi_{\tilde{\tau}}$ and $\mathcal{B}^+$ value. H_2O_2 is considered as an ignition precursor and it well characterises the identified region.
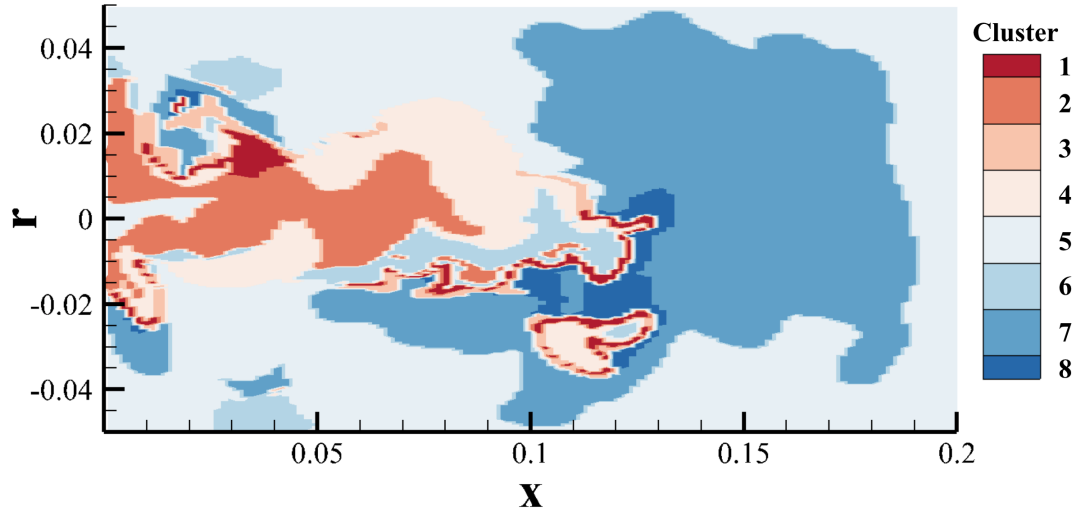
21

Figure 8: The local PCA map of clusters. The unit of the axes is m.

7. Conclusions

Turbulent partially premixed combustion under MILD condition inside a cylindrical combustor with aerodynamically established recirculation zone is studied using LES with the PaSR and EDC models for SGS combustion. The computed temperature and scalar mole fractions are compared to the measurements from [6]. A good overall agreement is observed for the PaSR model and it is comparable to those observed in past studies using FPV and homogenous reactor-based tabulation combustion models [9, 10]. The averaged temperature and CO_2 mole fractions are generally under-estimated, leading to over-estimation of O_2 mole fraction by the EDC, which could be due to the model parameters (e.g. C_γ) chosen or the value used for the canonical reactor residence time [27] since they are taken from past studies. Sensitivities of the EDC results to these parameters are to be explored in a future study. The LES data from PaSR model is analysed using TSR derived

22

from computational singular perturbation theory and convective-diffusive-reactive balance in T transport equation to identify ignition- and flame-like regions. A good agreement between these analyses are observed. Potential chemical markers (CMs) that can be used in laser diagnostics of MILD combustion are identified using local PCA.

Acknowledgments

References

[1] J. A. Wünning, J. G. Wünning, Flameless oxidation to reduce thermal NO-formation, Prog. Energy Combust. Sci. 23 (1997) 81–94.

[2] A. Cavaliere, M. de Joannon, MILD Combustion, Prog. Energy Combust. Sci. 30 (2004) 329–366.

[3] B. B. Dally, A. N. Karpetis, R. S. Barlow, Structure Of Turbulent Non-Premixed Jet Flames In A Diluted Hot Coflow, Proc. Combust. Inst. 29 (2002) 1147–1154.

[4] A. De, E. Oldenhof, P. Sathiah, D. Roekaerts, Numerical Simulation of Delft-Jet-in-Hot-Coflow (DJHC) Flames Using the Eddy Dissipation Concept Model for Turbulence-Chemistry Interaction, Flow Turbul. Combust. 87 (2011) 537–567.

[5] M. Graça, A. Duarte, P. J. Coelho, M. Costa, Numerical simulation of a reversed flow small-scale combustor, Fuel Process. Technol. 107 (2013) 126–137.

[6] A. S. Veríssimo, A. M. Rocha, M. Costa, Operational, combustion, and emission characteristics of a small-scale combustor, Energy and Fuels 25 (6) (2011) 2469–2480.

[7] M. Ihme, Y. C. See, LES flamelet modeling of a three-stream MILD combustor: Analysis of flame sensitivity to scalar inflow conditions, Proceeding Combust. Inst. 33 (1) (2011) 1309–1317.

[8] Z. Li, A. Cuoci, A. Parente, Large Eddy Simulation of MILD combustion using finite rate chemistry: Effect of combustion sub-grid closure, Proc. Combust. Inst. 37 (4) (2019) 4519–4529.

[9] J. Lamouroux, M. Ihme, B. Fiorina, O. Gicquel, Tabulated chemistry approach for diluted combustion regimes with internal recirculation and heat losses, Combust. Flame 161 (8) (2014) 2120–2136.

[10] C. Locci, O. Colin, J. B. Michel, Large Eddy simulations of a small-scale flameless combustor by means of diluted homogeneous reactors, Flow, Turbul. Combust. 93 (2) (2014) 305–347.

[11] S. H. Lam, D. A. Coussis, Understanding complex chemical kinetics with computational singular perturbation, Symp. Combust. 22 (1) (1989) 931–941.

[12] Y. Minamoto, N. Swaminathan, R. S. Cant, T. Leung, Reaction zones and their structure in MILD combustion, Combust. Sci. Technol. 186 (8) (2014) 1075–1096.

[13] N. A. K. Doan, N. Swaminathan, Autoignition and flame propagation in non-premixed MILD combustion, Combust. Flame 201 (2019) 234–243.

[14] A. Parente, J. Sutherland, B. Dally, L. Tognotti, P. Smith, Investigation of the MILD combustion regime via Principal Component Analysis, Proc. Combust. Inst. 33 (2011) 3333–3341.

[15] N. Kornev, H. Kröger, E. Hassel, Synthesis of homogeneous anisotropic turbulent fields with prescribed second-order statistics by the random spots method, Commun. Numer. Methods Eng. 24 (2008) 875–877.

[16] H. G. Weller, G. Tabor, H. Jasak, C. Fureby, A tensorial approach to computational continuum mechanics using object-oriented techniques, Comput. Phys. 12 (6) (1998) 620–631.

[17] A. Cuoci, A. Frassoldati, T. Faravelli, E. Ranzi, OpenSMOKE++: An object-oriented framework for the numerical modeling of reactive systems with detailed kinetic mechanisms, Comput. Phys. Commun. 192 (2015) 237–264.

[18] R. W. Bilger, S. H. Stårner, R. J. KEE, On reduced mechanisms for methane-air combustion in nonpremixed flames, Combust. Flame 80 (2) (1990) 135–149.

[19] Z. Li, R. M. Galassi, P. P. Ciottoli, A. Parente, M. Valorani, Characterization of jet-in-hot-coflow flames using tangential stretching rate, Combust. Flame 208 (2019) 281–298.

[20] F. P. Kärrholm, Numerical Modelling of Diesel Spray Injection, Turbulence Interaction and Combustion, Phd thesis, Chalmers University of Technology, Chalmers, Sweden, 2008.

[21] Z. Li, M. Ferrarotti, A. Cuoci, A. Parente, Finite-rate chemistry modelling of non-conventional combustion regimes using a Partially-Stirred Reactor closure: Combustion model formulation and implementation details, Appl. Energy 225 (2018) 637–655.

[22] I. R. Gran, B. F. Magnussen, A Numerical Study of a Bluff-Body Stabilized Diffusion Flame, Part 2: Influence of Combustion Modelling And Finite-Rate Chemistry, Combust. Sci. Technol. 119 (1-6) (1996) 191–217.

[23] M. Valorani, S. Paolucci, E. Martelli, T. Grenga, P. P. Ciottoli, Dynamical system analysis of ignition phenomena using the Tangential Stretching Rate concept, Combust. Flame 162 (8) (2015) 2963–2990.

[24] M. Valorani, P. P. Ciottoli, R. Malpica Galassi, S. Paolucci, T. Grenga, E. Martelli, Enhancements of the G-Scheme Framework, Flow, Turbul. Combust. 101 (4) (2018) 1023–1033.

26

[25] D. M. Manias, E.-A. Tingas, F. E. Hernández Pérez, R. Malpica Galassi, P. Paolo Ciottoli, M. Valorani, H. G. Im, Investigation of the turbulent flame structure and topology at different Karlovitz numbers using the tangential stretching rate index, Combust. Flame 200 (2019) 155–167.

[26] J. C. Sutherland, A. Parente, Combustion modeling using principal component analysis, Proceedings of the Combustion Institute 32 (1) (2009) 1563 – 1570.

[27] D. A. Lysenko, I. S. Ertesvg, Reynolds-averaged, scale-adaptive and large-eddy simulations of premixed bluff-body combustion using the eddy dissipation concept, Flow, Turbulence and Combustion 100 (3) (2018) 721–768.